HOSTED BY
ELSEVIER
Available online at www.sciencedirect.com
ScienceDirect
Resource-Efficient Technologies 1 (2015) 19–27
www.elsevier.com/locate/reffit

Research paper

Iron oxide-modified nanoporous geopolymers for arsenic removal from ground water

Dinesh Medpelli [a], Robert Sandoval [b], Laurie Sherrill [b], Kiril Hristovski [b], Dong-Kyun Seo [a,*]

[a] Department of Chemistry and Biochemistry, Arizona State University, Tempe, AZ 85287, USA
[b] The Polytechnic School, Ira A. Fulton Schools of Engineering, Arizona State University, Mesa, AZ 85212, USA

Received 17 June 2015; accepted 23 June 2015
Available online 22 July 2015

Abstract

Composite materials of hierarchically porous geopolymer and amorphous hydrous ferric oxide were produced and characterized as a new potentially cost-effective arsenic adsorbent. The arsenic removal capabilities of the iron (hydr)oxide (HFO) media were carried out using batch reactor experiments and laboratory scale continuous flow experiments. The Rapid Small-Scale Column Tests (RSSCT) were employed to mimic a scaled up packed bed reactor and the toxicity characteristic leaching procedure (TCLP) test of arsenic adsorbed solid material was carried out to investigate the mechanical robustness of the adsorbent. The best performing media which contained ~20 wt% Fe could remove over 95 μg of arsenic per gram of dry media from arsenic only water matric. The role of the high porosity in arsenic adsorption characteristics was further quantified in conjunction with accessibility of the adsorption sites. The new hierarchically porous geopolymer-based composites were shown to be a good candidate for cost-effective removal of arsenic from contaminated water under realistic conditions owing to their favorable adsorption capacity and very low leachability.

Keywords: Geopolymer; Hierarchically porous; Arsenic removal; Water purification

1. Introduction

Arsenic is one of the most frequently found contaminants found in many drinking water sources in small and rural communities all over the world. The largest population at risk among countries with known groundwater arsenic contamination is in Bangladesh, followed by the state of West Bengal in India [1–3]. Prolonged intake of arsenic contaminated drinking-water is known to cause dermal lesions such as hyper- and hypopigmentation, peripheral neuropathy, skin cancer, bladder and lung cancers and peripheral vascular disease [4]. Although arsenic can exist in (−3), (0), (+3) and (+5) oxidation states in the earth's crust, in natural waters, it is mostly present in the most oxidized (+5) state as arsenate (AsO_4^{3-}); however, under anaerobic conditions, it is likely to be present in the (+3) oxidation state as arsenite (AsO_3^{3-}) [5,6].

A number of technologies have been reported for treating arsenic from drinking water based on different treatment methods [5,7–9]. Among these technologies, the ones based on adsorption have demonstrated the greatest potential because of their cost effectiveness, versatility, and simplicity of operation and maintenance [10]. Adsorption based systems for treating arsenic from water typically employ metal (hydr)oxides such as ferrihydrite, iron (hydr)oxide (HFO), titanium dioxide, zirconium dioxide, hematite, and goethite because they have excellent selectivity for arsenic, which forms inner sphere complexes with the metal atoms in the sorbent through oxygen bridges [11,12].

The high adsorption capacity of the metal (hydro)oxides is directly related to available sorption sites with which arsenic can form these inner-sphere complexes. However, it is often misguidedly thought that high adsorption capacities and arsenic removal performance could only be achieved by increasing the available surface area without engineering the accessibility to the available sites. In this context, the porosity and pore size distribution of a media play even a more critical role in increasing the overall arsenic removal performance of the adsorbent [13–17]. The impact of media's pore related properties on its arsenic removal performance becomes

* Corresponding author. Department of Chemistry and Biochemistry, Arizona State University, Tempe, AZ 85287, USA. Tel.: +1-480-727-7789; fax: +1-480-965-2747.
E-mail address: dseo@asu.edu (D.-K. Seo).

http://dx.doi.org/10.1016/j.reffit.2015.06.007

especially significant in hybrid adsorbents. These hybrid media employ strong porous materials as a supporting platform for metal (hydr)oxide nanoparticles, which allow for high surface area, but cannot be utilized in pack bed configurations because of their size. In parallel, their aggregation leads to surface area reduction and structural instability, which consequently leads to operational problems because of attrition and nanomaterial leaching. To mitigate these problems, highly porous supporting materials such as mesoporous silica or granular activated carbon (GAC) have been proposed for metal (hydr)oxide nanoparticle impregnation [18–22]. However, no study has been conducted to clearly demonstrate that porosity and pore size distribution of the base media critically affect the metal (hydr)oxide nanoparticle hybridization process, and consequently the overall arsenic removal performance of metal (hydr)oxide hybrid media.

To address this knowledge gap, we report new highly efficient and yet potentially inexpensive class of arsenic adsorbents, which utilize porous geopolymer as a mechanically strong supporting material. Geopolymers are emerging class of ceramic-like materials that are gaining significant attention due to their unusual properties, such as high compressive strengths, good heat and chemical resistance, and low environmental impact during production. Beyond the conventional applications as building or refractory materials [23] or in immobilizing toxic wastes [24], new research efforts are being focused toward introducing porosity into the material and utilize them in catalysis [25] and drug delivery [26,27]. Recently, we introduced hierarchically meso/macroporous structure into the otherwise dense geopolymeric matrix following a simple and readily scalable synthetic methodology developed previously by some of the current authors [28,29]. A hierarchical pore structure is advantageous because the smaller mesopores can be easily accessed through the larger macropores, hence improving (1) accessibility of precursors used in in-situ metal (hydr)oxide nanoparticle synthesis; and (2) diffusion kinetics of contaminants to available sorption sites. Larger macro/meso-porosity allows for more uniform distribution of nanoparticles into the media with minimal reduction in effective pore volume, consequently leading to a greater number of available metal (hydr)oxide sorption sites for contaminants like arsenic [30]. Additionally, the larger porosity leads to smaller intraparticle mass transport limitations and improves the overall kinetic efficiency of the system [16].

In order to further quantify the role of the high porosity in arsenic adsorption characteristics, we (1) synthesized different nanoporous geopolymer base media by modifying synthesis conditions; (2) impregnated the geopolymer base media with HFO nanoparticles; (3) characterized the properties of both geopolymer base and HFO nanoparticle impregnated media; (4) conducted batch isotherm experiments to develop Freundlich isotherm parameters; (5) employed the pore surface diffusion model to screen the performance of the media in packed bed conditions; (6) conducted a Rapid Small Scale Column Test (RSSCT) with the best performing media to assess the effect of co-contaminant completion on arsenic removal capacity; and (7) conducted tests to assess the arsenic leaching potential of spent adsorbent media.

2. Experimental and modeling approach

2.1. Synthesis of nanoporous geopolymer material (base media)

In the first step of the synthesis, a potassium silicate solution was prepared by dissolving an appropriate amount of KOH pellets (Sigma Aldrich) in deionized water in a polypropylene cup placed in a water bath. A suitable amount of fumed silica (Cabot, CA-BO-SIL® EH-5) was then added into the KOH solution and the mixture was stirred with a Stir-Pak laboratory mixer for 30 minutes at 800 rpm to give a clear solution. The geopolymer resins were then prepared by mechanically mixing metakaolinite into the potassium silicate solution to form a homogenous fluidic liquid. The metakaolinite was produced in advance by calcining kaolinite ($Al_2Si_2O_7{\cdot}H_2O$, Alfa Aesar) at 750 °C for 10 h. Eight different samples were prepared by varying the amounts of water, K/Al ratio and Si/Al ratio (Table 1). The pH of the resins was about 14 for all the compositions. Canola oil (The J.M. Smucker Company, Crisco®), paraffin oil (Alfa Aesar) or a mixture of both oils (Table 1) was then added to the resin at a 1:1 oil-to-water volume ratio and mixed for an additional 15 minutes to give a homogeneous but viscous emulsion. The emulsion was transferred to a polypropylene cup and cured in a laboratory oven at 60 °C for 24 h. The cured monolithic product was then broken into small pieces (approximately $1 \times 1 \times 1$ cm^3) and subjected to Soxhlet extraction with n-butanol as a solvent. The resulting nanoporous geopolymer (base media) pieces free of organics were dried overnight in the lab oven maintained at 120 °C. Complete removal of organics was confirmed by CHN analysis and infrared spectroscopy (data not shown).

2.2. In-situ synthesis of iron (hydr)oxide (HFO) nanoparticles

The base media were ground and sieved into 30×40 US mesh particles sizes (425–600 μm). This media size range is reflective of typical particle sizes used in full scale packed bed configurations for water treatment applications [31]. Subsequently, the impregnation of the base media with iron (hydr)oxide nanoparticles was carried out through an incipient wetness impregnation technique in the steps: (i) base media was soaked in $FeCl_3{\cdot}6H_2O$ (Alfa Aesar) dissolved in methanol (2.0 M solution) for 24 h; (ii) the resulting particles were filtered and were heated at 85 °C in an ammonia/moisture saturated atmosphere

Table 1
Synthetic parameters of the base media.

Sample	Water content (mol%)	K:Al:Si	Oil used	Oil ratio
1	68	2:1:2	Canola/Paraffin	50%/50%
2	68	2:1:2	Paraffin	100%
3	73	3:1:2	Canola	100%
4	73	3:1:2	Canola/Paraffin	50%/50%
5	68	1:1:1.5	Canola	100%
6	68	1:1:1.5	Canola/Paraffin	50%/50%
7	68	1:1:1.5	Canola/Paraffin	33%/66%
8	68	1:1:1.5	Paraffin	100%

for 12 h in order to raise the pH within the pores and therefore induce the precipitation of Fe(III) as hydrous ferric oxide; (iii) precipitation was completed by further heating the particles in an oven maintained at 85 °C for 12 h before drying at 120 °C for 12 h; (iv) the by-products (co-precipitated KCl and NH_4Cl) were removed from the pores of the composite material by thoroughly rinsing with deionized water; (v) the resulting reddish brown particles soaked in Millipore water were ready for subsequent arsenic removal experiments.

2.3. Material characterization

Powder X-ray diffraction (PXRD) patterns of the finely ground samples were collected using a Siemens D5000 diffractometer (Ni-filtered Cu Kα radiation with a wavelength of 1.5406 Å, operated at 40 kV and 40 mA, VANTEC-1 position-sensitive detector) at a scan speed of 2.0°/min and a step size of 0.016° 2θ. The resolution of the VANTEC-1 position-sensitive detector was $2\theta = 0.008°$. Samples for scanning electron microscopy (SEM) were prepared by placing few pieces of the products on a SEM stub using a copper conducting tape. Samples were then gold coated for 100 s and were studied using SEM-XL30 Environmental FEG (FEI) microscope operating at 5 kV. For transmission electron microscopic (TEM) studies, colloidal suspensions of ground samples in ethanol were dried on to copper grids and were studied using JEOL TEM/STEM 2010F operating at 200 kV.

Specific surface and pore size distributions area were determined via nitrogen sorption with a Micrometrics ASAP 2020 instrument. Specific surface areas were estimated using Brunauer–Emmett–Teller (BET) equation, while pore size distributions were obtained using the Barrett–Joyner–Halenda (BJH) method assuming a cylindrical pore model. Bulk porosity of the media was determined by pycnometry [16].

The iron content of the media was determined by using Thermo Scientific iCAP 6300 inductively coupled plasma–optical emission spectrometer (ICP–OES). Prior to the analysis, solid samples were acid-digested using a CEM MARS 6 microwave reaction system in repeated heating steps at 180 °C for 30 min with sequential addition of required reagents. Specifically, 20–30 mg of catalysts was heated in the reactor first with 3 mL of concentrated HCl solution (34–37 wt%, ACS), and second with a mixture of 3 mL concentrated HNO_3 (67–70 wt%, ACS) and 0.5 mL of HF solution (48–51 wt%, ACS). The digests were later quenched with 5 mL of 4.5 wt% H_3BO_3 solution aided by the microwave reactor.

2.4. Screening of arsenic adsorption capacities under pseudo-equilibrium conditions

The removal capacities of the iron (hydr)oxide media were screened by conducting batch adsorption experiments in arsenate only ($C_{As\text{-}0} \approx 120$ µg/L) containing 5 mM $NaHCO_3$ buffered ultrapure water at pH = 7.6 ± 0.3. The contact time was 3 days, which was sufficient to establish pseudo-equilibrium conditions [32]. To obtain adsorption pseudo-equilibrium data and develop isotherms, a minimum of 8 reactors per media type were used with media doses ranging from 0.1 g/L to 11.6 g/L. The Freundlich isotherm model was used to characterize the adsorption capacity of the media and provide parameters needed for modeling with the pore surface diffusion model (Equation 9).

$$q = K \times C_e^{1/n} \tag{9}$$

where q is the adsorption capacity (mg adsorbate/g adsorbent), K is the Freundlich adsorption capacity parameter ((mg adsorbate/g adsorbent) × (L/mg adsorbate)$^{1/n}$), C_e the equilibrium concentration of adsorbate in solution (mg adsorbate/L), and $1/n$ is the Freundlich adsorption intensity parameter (unitless).

2.5. Pore surface diffusion modeling and rapid small scale column tests (RSSCTs) for comparison of continuous flow arsenic adsorption performance

Characterization data and Freundlich isotherm parameters were used to model the breakthrough curves of a fixed bed adsorber system packed with the different media and compare their performance in continuous flow mode. Details related to the modeling methodology and the Pore Surface Diffusion model (PSDM) are provided in the Supplemental Information. To assess the effect of competitive adsorption from contaminants typically found in ground water, a Rapid Small Scale Test was conducted with the best performing adsorbent in NSF 53 Challenge water matrix. The Rapid Small-Scale Column Tests (RSSCT) are typically employed to mimic the performance of a full scale fixed adsorber bed systems at laboratory conditions, employing only a miniscule fraction of sorbent, time, and testing water than needed by a full scale system [33]. The RSSCT breakthrough curve was compared with the corresponding PSDM predicted breakthrough curve for arsenic only model. Details related to the RSSCT test and NSF 53 Challenge water matrix are provided in the Supplemental Information. Arsenic was analyzed with graphite furnace atomic absorption spectroscopy (GF-AAS) using nickel as matrix modifier (Varian 50B with GTA-110 system).

2.6. Assessment of arsenic leaching potential of spent adsorbent media

To assess the arsenic leaching potential of spent adsorbent media, toxicity characteristic leaching procedure (TCLP) test was performed with the best performing media following standardized test procedure described by the U.S. Environmental Protection Agency (EPA) method 1311 [34]. Briefly, spent media was mixed with the TCLP fluid at of pH 4.93 ± 0.05 and agitated (speed, 280 ± 5 rpm) for 18 h using a mechanical shaker. The fluid was filtered using 0.45 µm filter and analyzed for arsenic with GF-AAS using nickel as matrix modifier (Varian 50B with GTA-110 system).

The Freundlich isotherm model was used to develop the isotherms because it allows for easy assessment of the favorability of the adsorption process and use of its parameters in the Pore Surface Diffusion Model (PSDM), which was used to assess the performance of the media in a full scale packed bed continuous flow configuration [15]. The analysis of arsenic

Table 2
NSF 53 water matrix used in the tests. Five millimolar (5 mM) $NaHCO_3$ was used to buffer the water matrix.

	Ion	Concentration (mg/L)	Form
1	As(V)	0.12	Na_2HAsO_4
2	ClO^{4-}	0.1	$KClO_4$
3	F^-	1.0	NaF
4	NO_3^-	2.0	$NaNO_3$
5	PO_4^{3-}	0.04	$NaH_2PO_4{\cdot}H_2O$
6	SiO_2	20	$Na_2SiO_3{\cdot}9H_2O$
7	Ca^{2+}	40	$CaCl_2$
8	Mg^{2+}	12	$MgSO_4{\cdot}7H_2O$
9	SO_4^{2-}	50	$MgSO_4{\cdot}7H_2O$

concentration was conducted using Varian Spectra 50B-GTA 110 Graphite Furnace Atomic Absorption Spectrometer. Parameters in Table 2 describe the water chemistry of NSF 53 Challenge water [35]. The Rapid Small-Scale Column Tests (RSSCT) were employed to mimic a scaled up packed bed reactor [33].

3. Results and discussion

3.1. Media characterization

In our previous work [28,29], we demonstrated that the hierarchical pore network with co-existing distinctive mesopores and macropores can be introduced into the otherwise dense geopolymeric material by templating with triglyceride oil. We also revealed that the pore characteristics of these hierarchically porous geopolymers can be controlled by adjusting the synthetic parameters. In this study, eight different nanoporous geopolymers (media **1**–**8**) were produced to generate different pore sizes/structures as shown in Table 3.

Prior to HFO impregnation, the untreated nanoporous geopolymer media **3** and **5** prepared by adding canola oil, or the media **1**, **4**, **6** and **7** prepared by adding a mixture of canola oil and paraffin oil exhibited mesoporosity as well as macroporosity. Mesoporosity can be seen from the N_2 sorption isotherms (Fig. 1a and b) and BJH desorption pore size distribution curves (Fig. 1c and d), and the corresponding pore properties are listed in Table 3. Isotherms of these base media shown in Fig. 1a and b resemble type IV isotherm typical of a material having mesopores. The fact that these isotherms do not saturate at partial pressure, $P/P_o \approx 1$ indicates the presence of macropores (pores wider than 50 nm) as well. The presence of broad range of mesopores which extend into the macropore region can be clearly seen in the BJH desorption pore size distribution curves plotted in Fig. 1c and d. Furthermore, Fig. 2a and b show SEM images of the base media **3** chosen as a representative example of **1**, **3**, **4**, **5**, **6** and **7**. Co-existence of mesopores and macropores is clearly evident from these SEM images. The material exhibits discrete spherical pores whose diameter range from about 5 to 40 μm (Fig. 2a). A closer look in Fig. 2b revealed that the pore wall separating the spherical pores has a finer structure throughout the matrix indicating the mesoporosity confirmed by N_2 sorption analysis.

On the other hand, untreated media **2** and **8** prepared by adding solitary paraffin oil exhibits only a macropore network as seen in N_2 sorption isotherm (Fig. 1a and b) and BJH desorption pore size distribution curves (Fig. 1c and d). Fig. 2c and d shows SEM images of the base media **2** as a representative example. Spherical macropores (20–50 μm) are clearly visible from Fig. 2c but a closer look at the pore walls revealed additional macropores of smaller size (~2 μm) in Fig. 2d. Transmission electron microscopy (Fig. 3a) revealed that all the base media without any exception consisted of a gel like nanostructure of the material which is made up of nanoparticles that are strongly fused together at their necks.

After HFO impregnation, all media had uniform reddish-brown color all over the sample including internal surfaces, which indicates homogeneous impregnation of HFO. Furthermore, all samples exhibited open mesopores and macropores as confirmed by N_2 sorption (Fig. 4) and scanning electron microscopic studies (Fig. 3c), respectively revealing that the pores are not clogged upon impregnation. BET surface area increased and mesopore diameter decreased for all the media without any

Table 3
Pore properties of the media before and after HFO impregnation along with iron content, zeta potential and arsenic adsorption capacity values.

Sample	BET surface area (m^2/g)	Mesopore volume[a] (cm^3/g)	Mesopore width[b] (nm)	Macropore volume[c] (cm^3/g)	Bulk density[d] (g/cm^3)	Bulk porosity[d] (%)	Fe content[e] (wt %)	Zeta potential (mV)	Q100 (μg As/g dry media)	Meso/Macro pore ratio (%)
	Base media; **HFO media**	Base media; **HFO Media**	Base media; **HFO media**							
1-Fe	42; **98**	0.28; **0.24**	26; **12**	1.21	0.69	67	19	6.0	268	20
2-Fe	8.0; **171**	0.05; **0.18**	30; **5.0**	1.18	0.73	64	17	5.2	559	15
3-Fe	58; **73**	0.80; **0.22**	53; **10**	1.45	0.59	65	20	7.4	954	15
4-Fe	50; **298**	0.39; **0.30**	39; **5.0**	1.22	0.65	67	24	6.8	295	25
5-Fe	59; **75**	0.38; **0.42**	28; **20**	0.85	0.78	66	14	5.5	449	49
6-Fe	75; **234**	0.42; **0.35**	20; **7.0**	0.88	0.81	63	18	7.5	467	40
7-Fe	56; **192**	0.43; **0.29**	26; **7.0**	0.96	0.80	62	17	6.7	369	30
8-Fe	24; **69**	0.10; **0.11**	19; **6.0**	1.31	0.70	69	20	8.2	233	8.1

[a] From the pores with width no larger than 150 nm in the BJH desorption pore distribution.
[b] 4(BJH desorption pore volume)/(BET surface area).
[c] (Total pore volume determined by pycnometry) − (BJH desorption pore volume).
[d] From total pore volume determined by pycnometry.
[e] From ICP-OES.

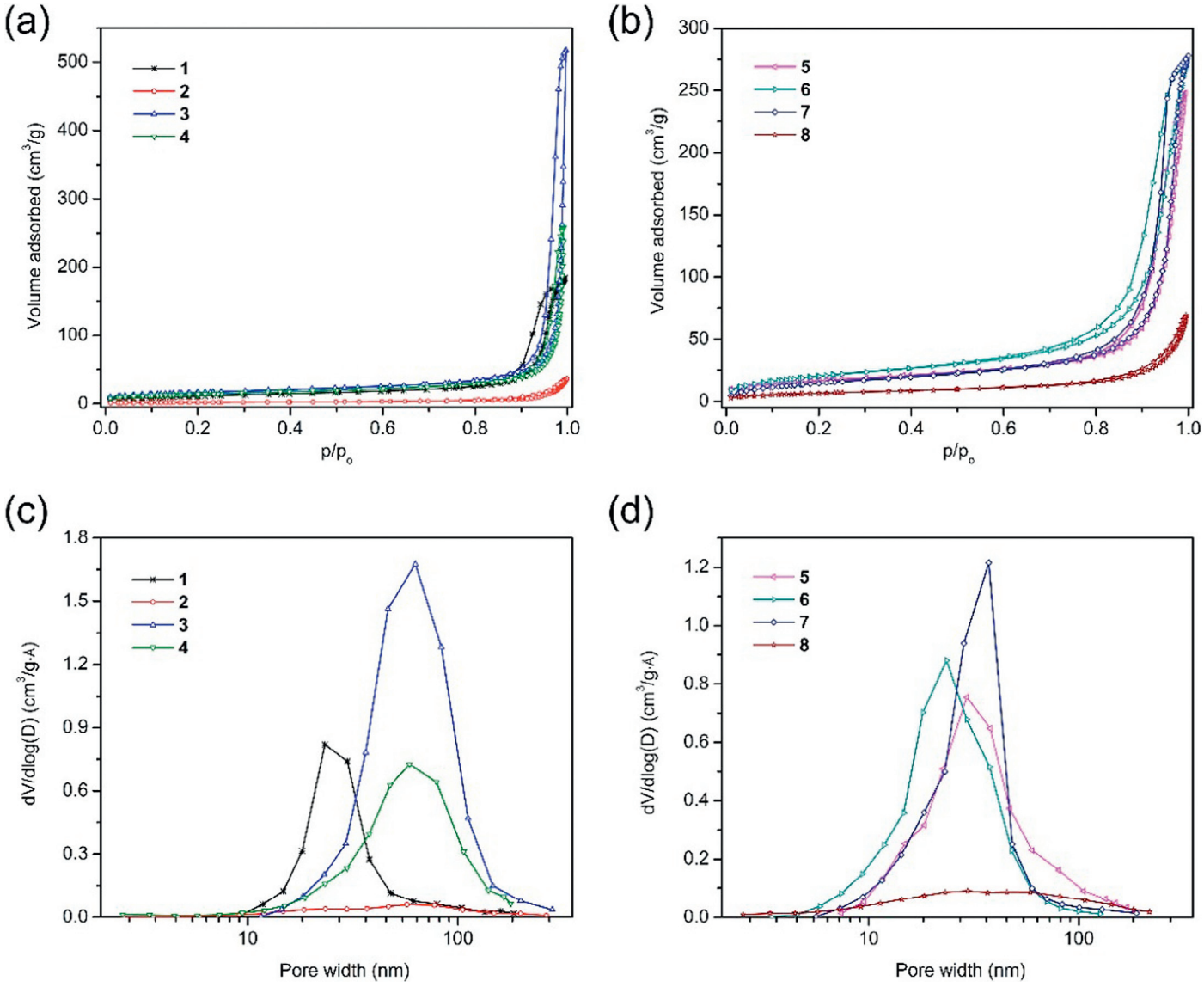

Fig. 1. Nitrogen sorption isotherms (a and b) and BJH desorption pore size distribution curves (c and d), respectively, of untreated media **1** – **4** (left) and **5** – **8** (right).

exception (Table 3), probably due to surface roughening of the pore walls, proving that HFO was successfully impregnated within the mesopores. A similar trend was reported by Bandyopadhyay et al. upon introducing TiO_2 nanoparticles into the pores of mesoporous MCM-48 by wet impregnation method [36].

Regarding to pore volume change after HFO impregnation, pore volume due to previously mesopores decreases but at the same time some of the macropores are reduced in size and start to contribute toward mesopore volume. Therefore, no clear trend in the mesopore volume change was observed. This was clearly noticed in media **2-Fe**, whose mesopore volume increased by more than three-fold from 0.05 cm^3/g to 0.18 cm^3/g upon HFO impregnation rather than decreasing. TEM studies of the media revealed that HFO is present as nanoparticles of approximate diameter of 4 nm (Fig. 3b), which explains the increment in surface areas upon impregnation. However, it is worth mentioning that the presence of bigger

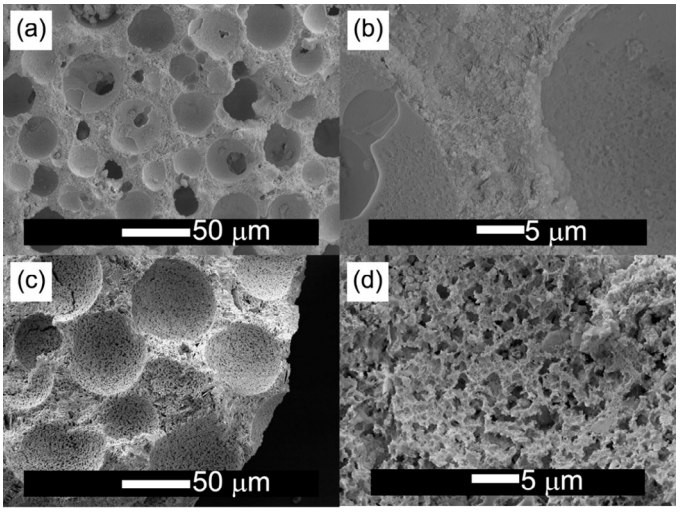

Fig. 2. SEM images of untreated media **3** (a and b) and **2** (c and d) as representative examples.

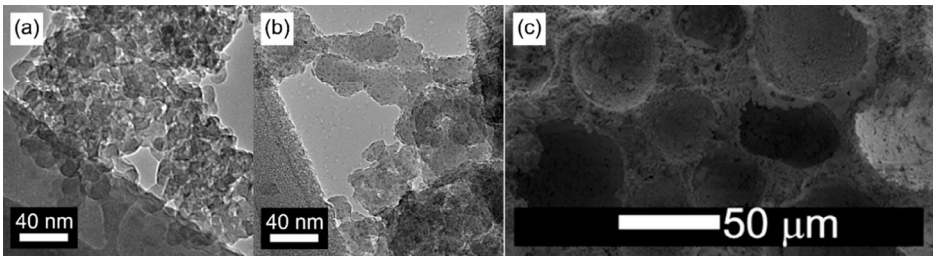

Fig. 3. TEM image (a) of untreated media **3**, and TEM (b) and SEM (c) images of HFO impregnated media **3-Fe**.

aggregates of HFO, particularly within the larger macropores, cannot be ruled out.

Fig. 5 shows the powder XRD pattern of media **3** before and after impregnation as a representative sample. Powder XRD analysis (Fig. 5) suggested that the impregnation yielded non-crystalline ferric species (hence amorphous hydrous ferric oxide or simply HFO). The base media themselves were amorphous and the largely featureless "hump" centered at approximately 27–30° in 2θ seen in their powder XRD patterns is the unique feature of geopolymers [37].

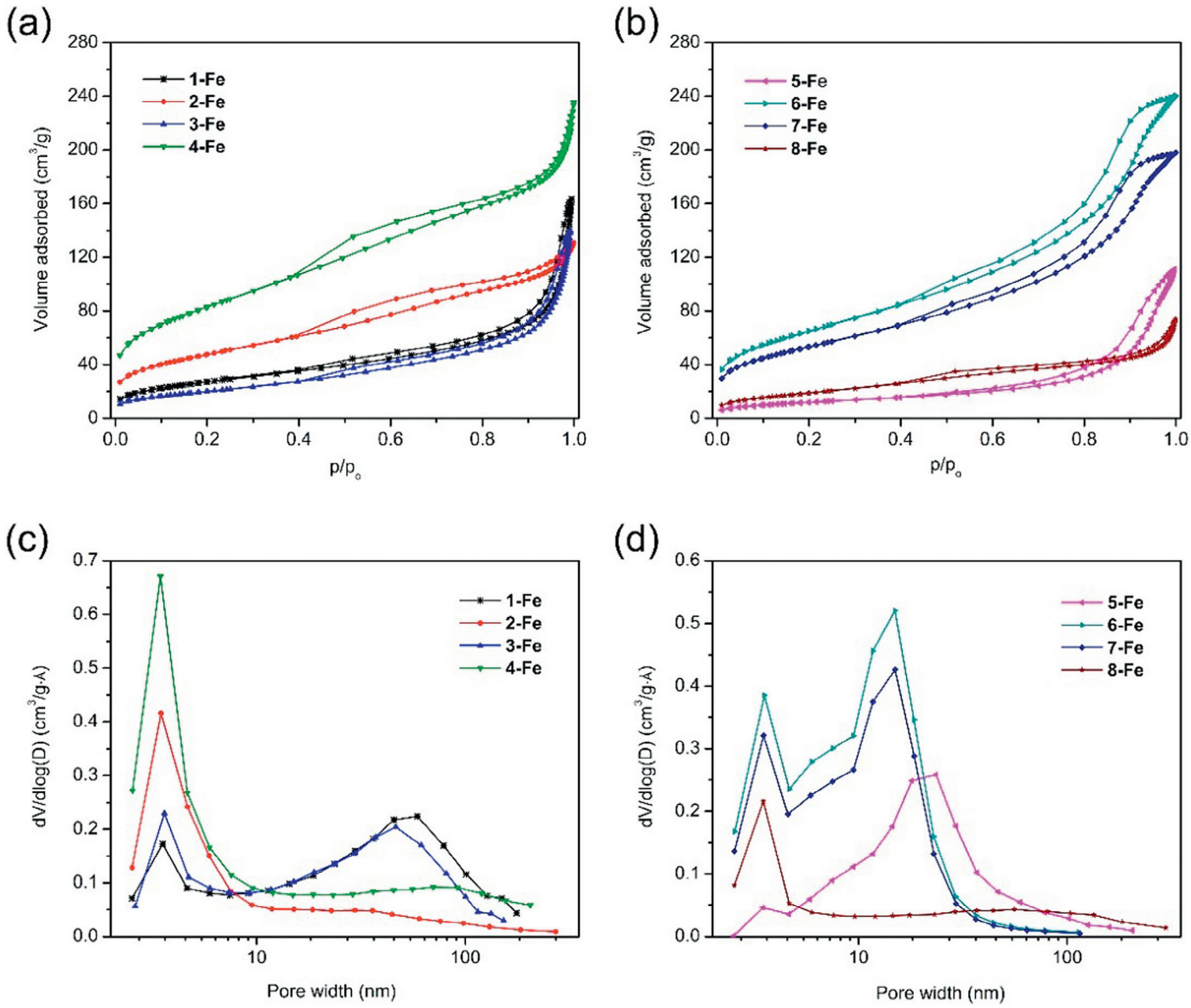

Fig. 4. Nitrogen sorption isotherms (a and b) and BJH desorption pore size distribution curves (c and d) of HFO impregnated media **1-Fe**–**4-Fe** (left) and **5-Fe**–**8-Fe** (right).

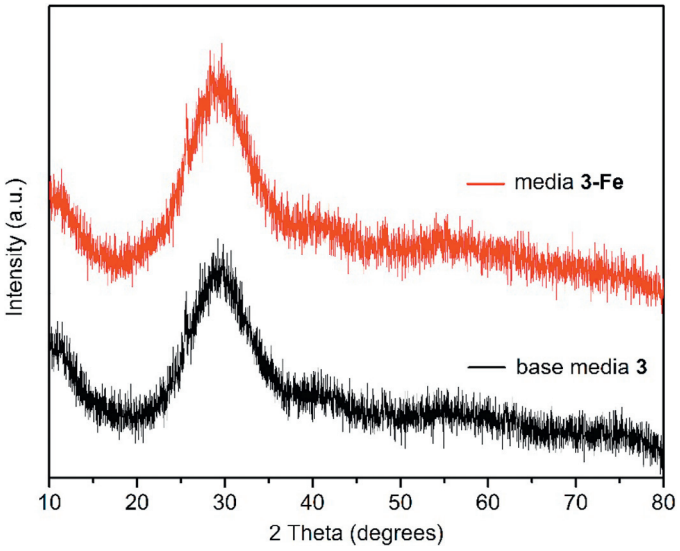

Fig. 5. Powder X-ray diffraction patterns of untreated media **3** (black) and HFO impregnated media **3-Fe** (red) as representative examples.

3.2. Comparing the arsenic adsorption capacities of the iron (hydr)oxide hybrid media

Fig. 6a illustrates the isotherms obtained from the batch reactor test data in arsenic only model water. All media exhibited Freundlich isotherm intensity (1/n) parameters ranging between 1.05 and 1.3, which suggests that these media may be suitable for treatment of waters exhibiting higher than typical arsenic concentrations. As illustrated in Fig. 6a, the **3–Fe** media exhibited highest adsorption capacity described by a $q_{100} \approx 950$ µg As/g media (Table 3). The **2-Fe** media was ranked second best performing with $q_{100} \approx 560$ µg As/g media, while the **6-Fe** and **5-Fe** media should be considered about the same and ranked third with $q_{100} \approx 450$ µg As/g media. Interestingly, however, none of these media exhibited the highest surface area after iron (hydr)oxide impregnation although this process created more surface area in all media as a result of the nanoparticle addition. Specifically, the best performing media 3-Fe had specific surface area of SA ≈ 73 m^2/g media. This was about 4 times less than 4-Fe which had SA ≈ 298 m^2/g, which also had the highest iron content. This clearly implies that fabricating media with high specific surface area and high metal (hydr)oxide content does not necessarily yield highest adsorption capacity because much of the metal (hydr)oxide may not be accessible for sorption of arsenic as a result of pore clogging during nanoparticle impregnation or in media with limited meso/macroporosity. In many cases, creation of highly mesoporous/macroporous media appears to be a more critical factor affecting adsorption of arsenic and similar oxyanions than creating media with high surface area, especially when such media is further impregnated with metal (hydr)oxide nanoparticles.

As illustrated in Fig. 6, the PSDM predictions further support this rationale. The 3-Fe media exhibited best performance, followed by 2-Fe and 6-Fe. However, the 5-Fe media, which was ranked the same as 6-Fe media, exhibited almost the worst performance. This media had the highest bulk density and the lowest macropore volume of the base material. The 5-Fe media was characterized by a rapidly increasing breakthrough curve, which is typical of media with unavailable adsorption sites. The 4-Fe media exhibited similar breakthrough curve as 5-Fe although it had much higher iron (hydr)oxide content i.e. more available adsorption sites, but not accessible. In contrast, the 3-Fe characterized with gradually increasing breakthrough curve, which is characteristic of pore diffusion dominated intraparticle mass transport, becomes the limiting transport mechanism due to diffusion of arsenic ions deeper into the particle to find available and accessible adsorption sites [38].

Since **3-Fe** media exhibited highest arsenic adsorption capacity in the arsenic only model water, it was further tested to

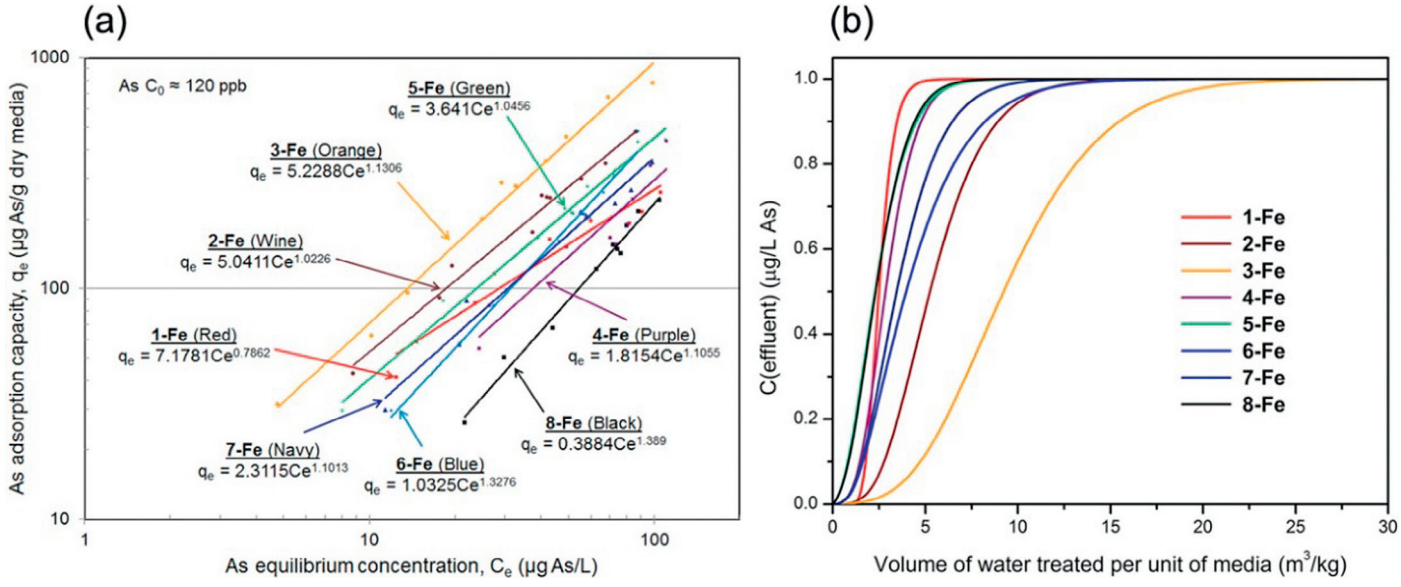

Fig. 6. Experimental isotherm data summary (a) and PSDM modeled breakthrough curves (b) of HFO media with arsenic only water matrix.

Table 4
Freundlich isotherm parameters for **3-Fe**.

Water matrix	Freundlich capacity parameter (K)*	Freundlich intensity parameter (1/n)	R^2	pH
As only water	5.23	1.13	0.989	7.6 ± 0.2
NSF 53 water	3.52	1.12	0.999	7.6 ± 0.2

$$* \frac{\mu g\ As}{g\ Dry\ media} \Big/ \left(\frac{\mu g\ As}{L}\right)^{1/n}$$

assess its performance in NSF 53 challenge model, water which is used to surrogate laboratory groundwater for assessing arsenic adsorption of media in realistic conditions. Batch experiments were conducted at the same experimental conditions, except for the change in the model water matrix, to assess the effect of the competing ions (silica and phosphate) onto the arsenic removal performance of the media. Table 4 summarizes the adsorption isotherm coefficients for **3-Fe** under equilibrium conditions with and without competing ions. The Freundlich intensity parameter (1/n) did not change when competing ions were introduced (1.13 versus 1.12, respectively), implying that the introduction of competing ions (silica and phosphate) did not affect the adsorption site energy. The lower Freundlich adsorption coefficient (K) is to be expected for the NSF 53 challenge model water because of the adsorption of the competing ions, which reduce the number available sites for arsenic to adsorb. The breakthrough curve for RSSCT conducted in NSF 53 challenge model water is presented in Fig. 7 together with a breakthrough curve modeled to mimic the same experimental conditions, except in arsenic only model water. The RSSCT was designed to mimic a scaled up packed bed reactor with characteristics presented in Supporting Information. The packed bed reactor provides a same breakthrough curve as the one experimentally obtained. Similarly, the modeled breakthrough curve that is presented for the RSSCT is identical to the modeled breakthrough curve for the packed bed reactor described in Supporting Information. Studies have validated the model for prediction of breakthrough curves in model waters with no competing ions, so no continuous flow column test was necessary in the arsenic only model water [15,33]. Both columns reached 95% breakthrough at approximately the same bed volumes (BV); however, the overall adsorption capacity of the media is lower in NSF 53 challenge model water.

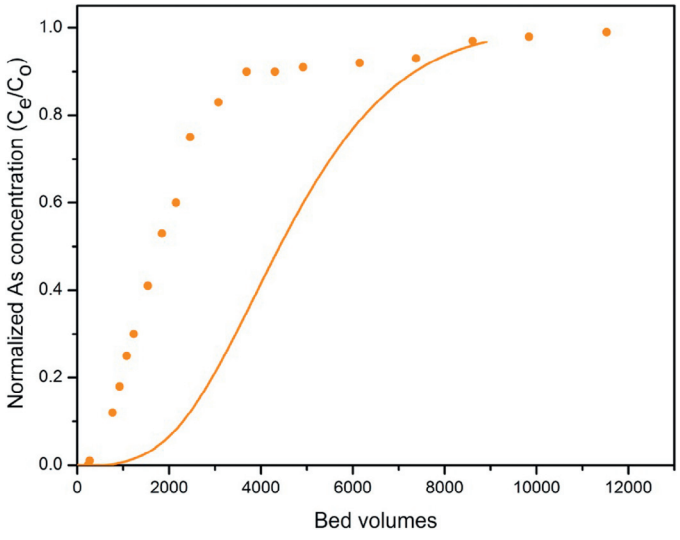

Fig. 7. Breakthrough curves for RSSCT with NSF 53 challenge model water (solid circles) and modeled RSSCT with arsenic only water (line) for **3-Fe**.

Table 5
Toxicity Characteristic Leaching Procedure (TCLP) results for spent **3-Fe**.

Sample	Initial pH	Final pH	As concentration (μg/L)	Standard deviation
Control	4.93	4.93	Not determined	-
3-Fe trial-1		5.36	44.4	1.49
3-Fe trial-2		5.38	43.3	1.35

TCLP As concentration = 43.9 μg/L.

In the absence of arsenic competing ions, the model predicted that approximately 2200 BV can be treated before a breakthrough of 10 μgAs/L is reached (C_e/C_0 ~ 0.085). The number of treated BV decreases by almost a factor of 3 as a result of ions with arsenic. Therefore, a packed bed reactor, as represented by the RSSCT, can treat about 700 BV before a breakthrough of 10 μg As/L is reached under realistic conditions. This difference in arsenic adsorption capacity is a direct result of the adsorption of competing ions (silica and phosphate). The high silica concentration causes rapid saturation of the available adsorption sites located near the outer layers of the media particle, which is illustrated by the rapid breakthrough in Fig. 6b. Then, the gradual breakthrough expected as the only available sites left for the arsenic and competing ions is deeper regions of the particle and the intraparticle mass transport is the limiting mechanism.

3.3. Assessing the arsenic leaching potential of spent adsorbent media

The stability of the spent adsorbent (spent **3-Fe**) was evaluated and its disposal options were examined by performing a Toxicity Characteristic Leaching Procedure (TCLP). TCLP determines the propensity of the selected media to leach arsenic after landfill disposal. In order for the media not to be labeled as hazardous, as defined in 40 CFR §26.24 Table 1, the waste media must meet the definition of toxicity for waste code D004 (arsenic), exhibiting an arsenic concentration less than 5 mg As/L [34]. Two samples of spent media from column testing, **3-Fe**, were tested to provide duplicate testing validation. Table 5 outlines the results of the TCLP tests. The arsenic concentration of the filtrate was determined to be about 44 μg As/L, 100× below the EPA limit of 5 mg As/L required to meet the toxicity characteristic. Based on the results, the spent media does not qualify as hazardous materials and can be disposed as a solid waste. This result is expected based on strong chemical bonding formed between arsenic species with developed media.

4. Conclusions

Composite materials of hierarchically porous geopolymer and HFO having high surface areas and interconnected meso/macropores were successfully developed via wet impregnation for the removal of arsenic from contaminated waters. X-ray studies indicate that HFO introduced into the pores is amorphous in nature and did not seem to alter the structure of the nanoporous geopolymers. It is concluded that the new hierarchically porous geopolymer-based composites can be good candidates for cost-effective removal of arsenic from contaminated water under realistic conditions owing to their favorable adsorption capacity and very low leachability. Research efforts to scale-up and further reduce the cost of production processes are undergoing and will be reported elsewhere. This study also opens up the ways to introduce various active species, such as catalysts and adsorbents into the hierarchically porous network of geopolymers and designing many more novel composite materials.

While all the media have shown arsenic removal capability with varying capacities, the comparative analysis of the different media characteristics clearly indicates that fabricating media with high specific surface area and high metal (hydr)oxide content does not necessarily yield highest adsorption capacity because much of the metal (hydr)oxide may not be accessible for sorption of arsenic as a result of pore clogging during nanoparticle impregnation or in media with limited meso/macroporosity. Rather, creation of highly mesoporous/macroporous media appears to be a more critical factor affecting adsorption of arsenic and similar oxyanions than creating media with high surface area, especially when such media is further impregnated with metal (hydr)oxide nanoparticles.

Acknowledgements

This work was supported by Mattium Corporation through NSF SBIR Phase II (Award Number 1152665). D.M.'s research assistantship was partially supported by the Center for Bio-Inspired Solar Fuel Production, an Energy Frontier Research Center funded by the U.S. Department of Energy, Office of Science, Office of Basic Energy Sciences under award number DE-SC0001016. We gratefully acknowledge the use of facilities within the LeRoy Eyring Center for Solid State Science at Arizona State University.

Appendix: Supplementary material

Supplementary data to this article can be found online at doi:10.1016/j.reffit.2015.06.007.

References

[1] M.M. Karim, Water Res. 34 (2000) 304–310.
[2] D. Da, A. Chatterjee, B.K. Mandal, G. Samanta, D. Chakraborti, B. Chanda, Analyst (Cambridge, U. K.) 120 (1995) 917–924.
[3] A. Chaterjee, D. Das, B.K. Mandal, T.R. Chowdhury, G. Samanta, D. Chakraborti, Analyst (Cambridge, U.K.) 120 (1995) 643–650.
[4] WHO (Press), Guidelines for Drinking-water Quality, *third ed.*, World Health Organization, Geneva, 2008.
[5] D. Mohan, C.U. Pittman Jr., J. Hazard. Mater. 142 (2007) 1–53.
[6] P.K. Dutta, A.K. Ray, V.K. Sharma, F.J. Millero, J. Colloid Interface Sci. 278 (2004) 270–275.
[7] C.K. Jain, R.D. Singh, J. Environ. Manage. 107 (2012) 1–18.
[8] P. Sylvester, P. Westerhoff, T. Moeller, M. Badruzzaman, O. Boyd, Environ. Eng. Sci. 24 (2007) 104–112.
[9] M. Gallegos-Garcia, K. Ramirez-Muniz, S. Song, Miner. Process. Extr. Metall. Rev. 33 (2012) 301–315.
[10] M. Jang, S.-H. Min, T.-H. Kim, J.K. Park, Environ. Sci. Technol. 40 (2006) 1636–1643.
[11] V. Lenoble, O. Bouras, V. Deluchat, B. Serpaud, J.-C. Bollinger, J. Colloid Interface Sci. 255 (2002) 52–58.
[12] D.B. Singh, G. Prasad, D.C. Rupainwar, Colloids Surf., A 111 (1996) 49–56.
[13] J. Elton, K. Hristovski, P. Westerhoff, ACS Symp. Ser. 1123 (2013) 223–236.
[14] K.D. Hristovski, P.K. Westerhoff, US Patent US20130175220A1, 2013.
[15] K.D. Hristovski, P.K. Westerhoff, J.C. Crittenden, L.W. Olson, Sep. Sci. Technol. 43 (2008) 3154–3167.
[16] K.D. Hristovski, P.K. Westerhoff, J.C. Crittenden, L.W. Olson, Environ. Sci. Technol. 42 (2008) 3786–3790.
[17] P.K. Westerhoff, K. Hristovski, Proc. the 230th ACS National Meeting & Exposition, IEC-171, 2005.
[18] X. Chen, K.F. Lam, Q. Zhang, B. Pan, M. Arruebo, K.L. Yeung, J. Phys. Chem. C 113 (2009) 9804–9813.
[19] Z. Gu, B. Deng, Environ. Eng. Sci. 24 (2007) 113–121.
[20] Z. Gu, J. Fang, B. Deng, Environ. Sci. Technol. 39 (2005) 3833–3843.
[21] X. Guo, F. Chen, Environ. Sci. Technol. 39 (2005) 6808–6818.
[22] K.D. Hristovski, P.K. Westerhoff, T. Moller, P. Sylvester, Chem. Eng. J. (Amsterdam, Neth.) 146 (2009) 237–243.
[23] P. Duxson, J.L. Provis, G.C. Lukey, J.S.J. van Deventer, Cem. Concr. Res. 37 (2007) 1590–1597.
[24] K. Komnitsas, D. Zaharaki, Miner. Eng. 20 (2007) 1261–1277.
[25] P. Sazama, O. Bortnovsky, J. Dedecek, Z. Tvaruzkova, Z. Sobalík, Catal. Today 164 (2011) 92–99.
[26] E. Jaemstorp, J. Forsgren, S. Bredenberg, H. Engqvist, M. Stroemme, J. Control. Release 146 (2010) 370–377.
[27] E. Jaemstorp, M. Stromme, G. Frenning, J. Pharm. Sci. 100 (2011) 4338–4348.
[28] D. Medpelli, J.-M. Seo, D.-K. Seo, J. Am. Ceram. Soc. 97 (2014) 70–73.
[29] D.-K. Seo, D. Medpelli, J.-M. Seo, US Patent 20130055924 A1, Mar 7, 2013.
[30] R. Sandoval, A.M. Cooper, K. Aymar, A. Jain, K. Hristovski, J. Hazard. Mater. 193 (2011) 296–303.
[31] D.R.U. Knappe, V.L. Snoeyink, P. Roche, M.J. Prados, M.-M. Bourbigot, Water Res. 31 (1997) 2899–2909.
[32] A. Jain, J. Sanner, R. Sandoval, K. Hristovski, ACS Symp. Ser. 1123 (2013) 205–222.
[33] P. Westerhoff, D. Highfield, M. Badruzzaman, Y. Yoon, J. Environ. Eng. 131 (2005) 262–271.
[34] Toxicity Characteristic Leaching Procedure, 40 Codes of Regulations, U.S. Environmental Protection Agency, Washington, DC, 1992; Part 261, pp. 31, 1992.
[35] K. Hristovski, P. Westerhoff, T. Möller, P. Sylvester, W. Condit, H. Mash, J. Hazard. Mater. 152 (2008) 397–406.
[36] M. Bandyopadhyay, A. Birkner, M.W.E. van den Berg, K.V. Klementiev, W. Schmidt, W. Grünert, et al., Chem. Mater. 17 (2005) 3820–3829.
[37] J. Davidovits, J. Therm. Anal. Calorim. 37 (1991) 1633–1656.
[38] G. Athanasaki, L. Sherrill, K.D. Hristovski, Environ. Sci. Water Res. Technol. (2015).